Computational investigating the combination of finned heat sink and phase change material as a cooling technology for a solar panel to be applied in arid areas

Ahmad Elamaireh, Jaydeep Goraniya, Madeleine L. Combrinck

Northumbria University, Newcastle-upon-Tyne, NE18ST, United Kingdom.

Abstract
This paper entails a computational investigation that aims to examine the effects of applying Phase Change Materials (PCM) and fins as a cooling technology for the Photovoltaic (PV) panel system in arid areas. In previous case studies, it is noticeable that PCM heat transfer showed to be a weak point, therefore, the focus of this investigation is to enhance the efficiency of the heat transfer between PCM and the ambient atmosphere by applying fins on the container of PCM. Enhancing the heat transfer helps PCM to remain in its transitional phase, which allows PCM to absorb latent heat (LH). The findings of this paper show the effects of combining PCM and fins, evidencing that it decreases the temperature of the PV panel's surface temperature around 7 K for a heat flux and the ambient temperature of 750 W/m^2 and 318.15 K respectively.

1. Introduction
The focus of generating power from sustainable and renewable sources has increased over the last two decades with the high potential of oil depletion. New technologies are being developed to assist in producing unpolluted energy, with renewable energy being the future of world energy producers because they rely on the natural sources, i.e. sun, wind and water. While each technology generates electricity from an individual natural source, for example, wind turbines work by utilizing the mechanical movement created from wind to generate electricity, a hydropower turbine generates electricity from the mechanical power within the water flow, similarly, the solar panel works by absorbing heat incidents on its surface and converts them into electrical energy.

Potential obstacles stand in the way of harvesting renewable energy effectively, regarding the wind turbine, the wind velocity is required to be within a specific range to allow the turbine blades to generate electricity efficiently [1]. Because of this, controllers are used to monitoring the turbine's blades to obtain the desired results. In a like manner, the photovoltaic works efficiently at 25 °C, but when the temperature increases, the efficiency starts decreasing [2]. Moreover, cell life can be degraded by high solar cell temperature, resulting in potential cell damage under extreme temperature [3]. Thus, intensive research has been conducted to investigate methods to cool down the photovoltaic surface temperature; these methods are

namely, passive or active. For instance, the active method could be the mist water cooling system and water film cooling system [4]. However, the passive method is implemented in such systems more often due to a lower operational cost and higher energy density [5]. The techniques of the passive cooling method are namely, Hybrid PV/T system, Micro-channel cooling system, Thermo-electric cooling system, Heat pipe cooling system.

A finned heat sink (FHS) is another example of cooling system which efficiently absorbs heat from the surface. It then cools and transfers this heat to the ambient conditions [2]. In some studies, introducing an FHS it significantly reduces the cell temperature, consequently affecting the PV cell efficiency [6].

Furthermore, phase change materials (PCM) are a powerful mean to absorb and store temperature in the form of sensible and latent heat. The sensible heat is absorbed and stored in its solid phase; this phase starts at the beginning of the operation period when the temperature is lower than the fusion point. Once the material reaches the transitional phase temperature, the latent heat (LH) becomes stored within the material.

The higher PV cell temperature results in a reduction of the electricity produced. Therefore, arid areas are the most affected due to lack of sources (i.e. Water.) to cool down the PV cells surface temperature because of the temperature being notably higher. Following this, an investigation has been conducted on the combination of FHS and PV cell; the results showed a 10 °C decrease of the PV cell surface temperature [2]. Likewise, another experiment has been implemented on a concentrated solar cell to find out the influence of PCM on the surface temperature of PV cell; the results showed the PV cell temperature had reduced by 15 °C in comparison with the naturally cooled system [3]. These two technologies show promising results working appropriately as a cooling technology, especially if they are combined and used in harsh conditions; this is concluded by the computational analysis of PCM and fins. The findings show that the combination of PCM and FHS reduces the solar panel surface temperature significantly [6]. From some recommendations in this area, there are suggestions for an enhancement of the container of PCM to improve the heat transfer between the PCM and the outside atmosphere [7].

2. Previous studies

The surface temperature of PV cells plays a crucial role for the efficiency and subsequently generated energy from PV, while the exposed PV panel converts 20% of the incident radiation, and the rest is converted into heat. Whereas the photovoltaic principles can be explained briefly as follows; the photon from the insolation is absorbed by exciting electrons in P-N junction, then the charge-carriers start moving from the valence band towards the conduction band, through this process the electricity is generated [8]. However, because not all of the radiation is used in this process, the exceeded heat starts overheating the PV temperature, which results in a reduction of the output electricity, so some technologies have been investigated in order to mitigate it and improve the system.

Cooling technologies for PV panels have been the main focus to be improved to harvest more electrical energy, and in some cases, to exploit thermal and electrical energies from these systems. Some technologies rely on extracting the heat from PV cells and apply it for other purposes; in this case, hybrid PV/Thermal is an excellent example to be mentioned. While this system contains a thermal collector placed on the back of PV panel, the operating mechanism is based on dissipating the exceeded heat from PV panels and utilized to heat up the heat removal fluid, while the latter is utilised for domestic application such as space heating, preheating water or ventilation. This way allows recovering a significant amount of wasted energy [9]. Similarly, [10] have implemented microchannel-cooling technology; this technology encompasses on micro heat exchangers where the coolant fluid flows on the side of the device to dissipate the generated heat by the electronic device. The coolant fluid runs between electronic components and the external heat exchanger, which uses the forced convection to remove the heat in the fluid.

Kane and Verma, [11] have examined thermoelectric cooling systems, which are composed on n-type and p-type semiconductors. The components are connected electrically in series, but thermally in parallel. The photon carriers absorb the heat, which causes a commotion, making them move from the hot side to the cold side, this process results in a voltage and current. Conversely, a sufficient heat pump starts cooling one side and heating up the other one; the effective heat pump is caused by an applied voltage which makes the current run through the materials. A heat sink is connected to the hot side to dissipate the temperature to the ambient. The water film cooling method is another technology used to cool down PV cells surface temperature; this method is one of the active methods, which mainly uses water to decrease the temperature, while the water is driven over the PV panel surface. Besides that, the reflection is minimized which means the performance of PV cells will improve [12].

From the existing cooling technologies in the literature, it can be concluded that the low heat transfer rates causes limited effectiveness. Therefore, more functional cooling technology is essential. Accordingly, PCM technology is another method has attracted the scholars' attention. Whereas, this method is used to dissipate the undesired heat from PV panel; therefore, it is considered as a promising technology that is due to its ability to provide appropriate heat extraction cost-effectively.

Thermal energy is categorized as sensible heat storage (SHS) and LH thermal energy storage (LHTES). While the energy storage is considered as a dependable mean to improve the reliability and the performance of the energy generator systems, for example, it is used to boost the effectiveness of solar panel by absorbing the exceeded heat from PV surface.

With this in mind, Phase Change Materials (PCMs) are used to conserve the energy, which comes in several forms. The category of thermal energy storage that used in (PCM) is illustrated as follows:

- Before the PCM transformation stage, sensible heat starts warming up the PCM temperature while the phase in this stage is either solid or liquid. The amount of sensible heat stored in the PCM depends on the SH of the PCM, the temperature variation and the amount of storage material [13].
- On the contrary, LHTES is stored during the conversion phase period namely; solid-liquid, solid-solid or liquid-gas and inversely. While the given equation is for the storage capacity of LHS system with a PCM setting:

$$Q = \int_{Tm}^{Ti} mC_p dT + ma_m \Delta h_m + \int_{Tm}^{Tf} mC_p dT \qquad (1)$$

where a_m is the fraction of PCM melted, Δh_m is the heat of fusion of PCM per unit mass, and m is the mass of a PCM [13].

Regarding practical research, [14] led the way towards experimental research concerning linking PV cells with PCM as an integrated system. However, the weak thermal conductivity and minimal connection area caused temperature dissimilarity along the panels. Conversely, this improved later by introducing copper containers and an aluminium absorber.

Ma et al. [7] utilized PCM technology on a V-trough PV, a tiny pad of PCM was located on the rear of PV panel, the experiment involved two parts, interior and exterior. The interior part of the experiment showed that the temperature with the PCM remained at 65-68 °C for three hours, however with the absence of the PCM the temperature accelerated to 90 °C in 15 minutes. Exterior results displayed that the system's temperature declined from 78 °C to 62 °C throughout the time span of the day. The obtained results showed that the total system power was boosted one and half time over with a self-sufficient system. The significance of the research by [15] suggests to the importance of combining metal fins into the PCM container. Their study's conditions were at 1000 (W/m²) radiation and ambient temperature of 20 °C, with a PCM of fusion temperature 32 °C inside two fins. It was found that to keep the panel's temperature around 25 °C; the PCM fusion temperature should be close to the surrounding temperature.

Upon further understanding, PCM cannot sustain the temperature mitigated for an extended period, which is due to the unfavourable characteristics of the PCM, which is the low thermal conductivity, resulting in low rates of phase change progression and weak effectiveness of thermal energy storage and absorption. Subsequently, the feebleness of thermal conductivity results in insufficient heat exchange between the PCM and the environs to extend the period of mitigation temperature, suggesting that an improvement is required. As it is featured in the published articles, the utilization of an extended surface such as fins is commonly used to enhance the heat transfer [16].

Tan [3] undertook an experimental investigation centred around concentrated solar power; the findings suggested that PV-PCM system enhanced 5% of the power yield and decreased the temperature by 15 °C. noticeably, the system potentially would lose more temperature by introducing fins in the PCM container, proving what [17] inferred from their experiment.

An experimental and computational study was conducted by [18], which involves of PCM surrounding a longitudinal fin, where they lie inside a cylindrical vertical tube. The results of the study show that the relation between the number of fins and the time needed to complete the solidification process is inverse, which is expressed as 1/n; where n is the number of fins. However, a possible drawback is doubted, which is the difficulty of fixing the fins inside the tube. Therefore, a case study was directed by [19] about considering the outer surface of PCM to be used for applying fins and thermal heat fluid on it, and with a larger tube surrounding these configurations. The results indicated to a specific increase of the solidification rate with the increase of the number of fins, while the fins thickness shows a negligible effect.

Other case study shows that the influence of fins thickness improves the heat transfer twice higher than the non-finned tube. Chan et al. [20] implemented the experimental setup with sodium acetate trihydrate ($CH_3COONa._3H_2O$) as PCM, and his central focus was on the effects of inlet temperature and the flow rate of heat transfer fluid (HTF) on heat transfer coefficient for the period of the solidification phase.

Stritih, [21] examined the thermal characteristics of LHTES for paraffin as PCM in the presence of fins, and without it, the results show a reduction in the solidification time around 40% in comparison with the absence of fins. Moreover, it was noted that the natural convection was dominant during the melting process. Furthermore, it was found that the influence of fins on the melting rate was unimportant, whereas the conduction was prevailing the heat transfer in the solidification process. Concerning the effects of fin configuration and functioning parameters, [22] had investigated their role on the solidification and melting phase in FHS and exchanger for RT35 as PCM. From the obtained results, it is concluded that the melting time decreases when the water flow side regime is turbulent due to the increase of the turbulence of heat transfer coefficient. This shows us that by adding fins to the model affects the solidification time notably when compared with the melting period.

Alternatively, another group of investigations have been conducted on unsteady flow, in this case, [23] have implemented a CFD and experimental study on the attitude of heat transfer under unsteady flow in a symmetrical fractal silicon microchannel. The results displayed that the heat transfer rate improved by 25-40% for the frequency of (2-10 and 30-40 Hz) and was higher than the frequency (10-20 HZ) while the Re number remained stationary. Yu et al. [24] carried out a numerical investigation into improving the heat transfer using actuated plates through the insertion of the plates into the heat sink channels. The results showed that 61% was the maximum enhancement by agitation; besides, an increase of heat transfer rate was noticed when the frequency of the agitator plate increased. This shows a significant rise in heat transfer on the base surface as the sizing tip gap between the actuated plate and channels decreased; conversely, the heat transfers on sidewalls did not affect.

Li et al. [25] have experimented the influences of fins dimensions on the thermal behaviour of the vapour chamber of Flat-plate fin heat sink (FPFHS). A comparison was made between aluminium and vapour chamber heat sink; the findings showed that the vapour chamber played a vital role in reducing the maximum temperature and distributing the heat transfer uniformly on the base substrate. Lin et al. [26] tested the novel procedure to evade from the flow resistance by increasing the number of fins to increase the heat transfer area; however, the proposed design contains an oblique fin. The design showed a reduction of 6 C° and a higher acceleration of flow between the fins in comparison with the conventional vertical design. Moreover, the new design yielded better performance than the vertical fins with respect to the low flow rates. Hasan [27] has investigated several shapes of pin fin microchannel heat sink (PFMCHS) with nanofluids. The use of nanofluids, instead of water, shows an improvement with regards to heat transfer, especially when increasing the concentration of the nanofluids. In the same study, circular pin fins outstrip on the other shapes by increasing the heat transfer rate, while for the square pin-fins pumping power was recognized to be a higher number.

With the above studies in mind, three geometric configurations have been selected for analysis. The first case is a PV container without temperature mitigation techniques, while the second case will add PCM in the container. The third case simulated here will add the FHS to the bottom of the container to ascertain the extent to which it is affecting temperature management inside of the system.

3. Methodology

3.1 Assumptions

These following assumptions are considered in this case study:

- The airflow is laminar, as the airflow over the panel is not considered in this case.
- Heat transfer is achieved through convection and conduction.
- The PCM in the liquid phase is a Newtonian fluid [28].
- Heat transfer coefficient of the air is 50 W/m^2K.
- Solar heat flux and the ambient temperature are 750 W/m^2 and 318.15 K, respectively.
- Photovoltaic materials and their properties are same as [29].
- The system can be analysed using the base geometry and configuration of [29].

3.2 Phase change material selection

Concerning the PCM selection, the material should have the appropriate properties. According to [16], Calcium nitrate tetrahydrate matches the desired melting temperature 315.85 K. The SH properties were taken from a case study by [30], while the thermal conductivity was calculated from the equations obtained from experimental data, which had been conducted by [31], the equations are as follows:
For the solid phase:

$$ks \left(\frac{W}{mC}\right) = \ \ 0.43 + 0.001\ t, \ -20\ °C \leq \ t \leq \ 42.7\ °C \tag{2}$$

For the liquid phase:

$$Kl \left(\frac{W}{mC}\right) = \ \ 0.335\ +\ 0.001\ t, \ \ \ 42.7\ °C \leq \ t \leq \ 95\ °C \tag{3}$$

The density data was obtained from the linear function that is formed from several cases study that have been conducted on the density of Calcium nitrate tetrahydrate; the data showed agreement within the findings [32], the equation is as follows:

$$\rho l \left(\frac{g}{cm^3}\right) = 1.7683 - 7.558 * 10^{-4} * t, \ \ \ 10\ °C \leq \ t \leq 90\ °C \tag{4}$$

Other properties were found in the open literature, such as the viscosity (0.0669 kg/ms), molecular weight (236.149 g/mol.), enthalpy (36600 J/mol) and LH fusion (144 J/g) [32].

3.3 Validation

The validation case was implemented to compare the current settings with another case that has been previously done to ensure that the sets used are reliable and work correctly. For this instance, the boundary conditions and sets of [29] case studies were used to confirm the verifications, although not all adjustments could be acquired from the article or open literature, i.e. the PCM properties. In this event, a different PCM with similar properties was used as an alternative. While this can be observed 0.68% accuracy by validating results w.r.t temperature, the qualitative results of the validated case show correspondence with the original case.

3.4 Computational fluid dynamics (CFD) analysis

CFD modelling embodies a mathematical approach to solve the governing equations of fluid flow; the equations are differential equations. Mesh cells represent these equations, which each cell calculates the equations using finite-volume algorithm.

3.4.1 Governing equations

The Newtonian fluid is governed by correlations of fluid flow describing the momentum, conservation of mass and energy in Cartesian coordinated regime, the model in this case study is 2D, therefore the z dimension is removed from the governing equations as it is not used for the calculations, the equations are explained as follows:

The conversation of mass:

$$\frac{\partial \rho}{\partial t} + \frac{\partial (\rho u)}{\partial x} + \frac{\partial (\rho v)}{\partial y} = 0 \tag{5}$$

Where u and v are the velocity components in the x and y-directions, respectively.

The conversation of momentum:
The Y-direction encompasses the buoyancy forces, while the conservation of momentum lies in the Cartesian coordinate, the following equations are X-momentum and Y-momentum:

x-momentum:

$$\frac{\partial}{\partial t}(\rho u) + \frac{\partial}{\partial x}(\rho uu) + \frac{\partial}{\partial y}(\rho vu) = -\frac{\partial P}{\partial x} + \mu\left(\frac{\partial^2 u}{\partial x^2} + \frac{\partial^2 u}{\partial y^2}\right) \tag{6}$$

Where t is the time, ρ is the density, P is the pressure, and μ is the dynamic viscosity.

y-momentum:

$$\frac{\partial}{\partial t}(\rho v) + \frac{\partial}{\partial x}(\rho uv) + \frac{\partial}{\partial y}(\rho vv) = -\frac{\partial P}{\partial y} + \mu\left(\frac{\partial^2 v}{\partial x^2} + \frac{\partial^2 v}{\partial y^2}\right) - \rho g\beta(T_\infty - T) \tag{7}$$

Where g is the gravity acceleration, β is the coefficient of thermal expansion, T is the ambient temperature, and T_∞ is the surface temperature. Since $-\rho g\beta(T_\infty - T)$ is the buoyancy force given by the Boussinesq approximation and $\frac{\partial P}{\partial y}$ is from Darcy's law as accessible in [33]. As the flow is laminar, then $\frac{\partial P}{\partial y}$ is equal $\frac{-C(1-B_1(T))^2}{B_1(T)^3} \cdot \vec{u}$.

Conservation of energy:

$$\frac{\partial}{\partial t}(\rho c_P T) + \frac{\partial}{\partial x}(\rho u c_P T) + \frac{\partial}{\partial y}(\rho v c_P T) = k\left(\frac{\partial^2 T}{\partial x^2} + \frac{\partial^2 T}{\partial y^2}\right) + \acute{q} \tag{8}$$

Solidification/melting equations:
Equation 9 is applied to calculate the changes in Calcium nitrate tetrahydrate thermo-physical properties that happen through the phase transition [28].

$$B_0(T) = \begin{cases} 0, & T < (T_m - \Delta T) \\ \dfrac{T - T_m + \Delta T}{2\Delta T}, & (T_m - \Delta T) \leq T < (T_m + \Delta T) \\ 1, & T > (T_m + \Delta T) \end{cases} \tag{9}$$

Since B_0 is the liquid fraction of the PCM, T_m is the melting temperature, and ΔT is the half range of the melting temperature. B_0 rises from zero to one, as zero indicates to the solid phase and one to the liquid phase.
Whereas B_0 is estimated by a second order differentiable equation B_1. B1 (T) is the sixth-degree polynomial whose seven coefficients are calculated using the following conditions:

$$\begin{cases} B_1(T_m - \Delta T) = 0 \,; \; B'_1(T_m - \Delta T) = 0; \\ \quad B''_1(T_m - \Delta T) = 0; \; B_1(T_m) = 0.5 \\ B_1(T_m - \Delta T) = 1; \; B'_1(T_m - \Delta T) = 0; \\ \quad\quad B''_1(T_m - \Delta T) = 0 \end{cases} \tag{10}$$

The first and the second are derivatives of B_1 are B_1' B_1'' respectively, the outcomes of B_0 (T) and B_1 (T) are similar, but the dissimilarity is B_1 a second order continuously differentiable function. Calculations of the thermos-physics properties are dependent on B_1, which is seen in the next equations:

$$\begin{aligned} \rho(T) &= \rho_{solid} + (\rho_{liquid} - \rho_{solid}) \cdot B_1(T) \\ k(T) &= k_{solid} + (k_{liquid} - k_{solid}) \cdot B_1(T) \\ C_p(T) &= C_{psolid} + (C_{pliquid} - C_{psolid}) \cdot B_1(T) + L_F \cdot D(T) \end{aligned} \tag{11}$$

where: ρ is the density, k is the thermal conductivity and C_p is the SH includes the LH term (L_F) of fusion absorbed during the melting process. Whereas the smoothed delta Dirac that can be calculated from the following equation:

$$D(T) = \frac{e^{(-T(T-T_m)^2)/(\Delta T^2)}}{\sqrt{\pi \cdot \Delta T^2}} \qquad (12)$$

D is zero throughout all terms except in duration $[T_m - \Delta T, T_m + \Delta T]$, it is reasonable to allocate the LH similarly for the mean melting point.

3.4.2 Geometry Specification
The geometry of the models in this case study was designed in ANSYS Design Modellers. This paper is investigating the combination of PCM and FHS so that a comparison will be made between three models; abstract PV panel (Case 1), PV panel with PCM (Case 2) and PV panel and PCM and FHS (Case 3).

3.4.2.1 Case 1 Geometry
The geometry of the first case is identical to the models in [29] but without PCM material.

3.4.2.2 Case 2 Geometry
The geometry of the second case is based on [29] but includes the PCM materials, which are the PV panel (same components as the first case) and the container which is surrounding the PCM. The container is modelled with Aluminum and at a thickness of 5 mm around the PCM and high 5.9 mm. The aluminum layer was kept between a Tedlar layer and PCM, as it remains the heat is distributed along the PV panel.

3.4.2.3 Case 3 Geometry
This design has the same dimensions as the previous one, but the fins were added to it as their dimensions are in Table 1 according to the optimisation investigation that was implemented as discussed in section 3.5.

Table 1. Dimensions and properties of the fins.

Property	Quantity	Unit
Number of fins	37	
Thickness of individual fin	0.002	m
Spacing between fins	0.0049	m
Fin height	0.04	m

3.4.3 Mesh Resolution
The second step of establishing a CFD model study is the meshing process, as the mesh cells are typically the blocks of the CFD study, whereas each mesh cell is representative of the governing CFD equations. Therefore, this section will discuss the appropriate procedure of creating the mesh within this case study and the grid refinement study. ANSYS software has developed an innovative mesh designer, which is the one used in this investigation. After creating the geometry, the Meshing modeller was used to create the mesh; several meshes were generated to enable the study of the grid independence.
In this section, the number of elements and nodes of the chosen models are presented in the Table 2.

Table 2. Number of elements and nodes per case.

Property	First Case	Second Case	Third Case
Number of elements	13750	115660	135991
Number of nodes	17528	121093	145189

3.4.3.1 Grid Refinement study
By implementing a numerical study, the major problem that arises is choosing the appropriate mesh size and resolution. Grid refinement study (grid-independent) is the approach that can predict the readings at

zero grid spacing and the percentage of the errors. This study comprises Richardson's extrapolation and grid convergence index (GCI).

It was examined on the flat model of PV cell and the container of PCM to see the symmetrical behaviour and to test the temperature manner on the top layer of the PV cell. While the three mesh models give different results, Richardson's extrapolate method was implemented in order to distinguish the appropriate mesh. As Richardson's extrapolation is a method that estimates the results at zero grid spacing [38], the value at zero grid spacing can be calculated from the following equation:

$$f_{h=0} \cong f_1 + \frac{f_1 - f_2}{r^p - 1} \tag{13}$$

Since r is the refinement ratio between the models, it is calculated from the following equation:

$$\frac{h_2}{h_1} \tag{14}$$

While the order of convergence p is calculated from the next equation:

$$\ln(\frac{f_3 - f_2}{f_2 - f_1})/\ln(r) \tag{15}$$

From Table 3, which shows the results of each of the grid at increasing fineness level, the results of the grid independence study can be calculated:

Table 3. Number of elements and nodes per case.

Grid	Grid spacing	Temperature [K]
1 - Fine	2	326.653
2 - Medium	4	326.284
3 - Coarse	8	325.889

The refinement ratio:

$$r = \frac{8}{4} = \frac{4}{2} = 2 \tag{16}$$

While the order of convergence equals:

$$p = \ln\frac{\frac{325.889 - 326.284}{326.284 - 326.653}}{\ln(2)} = 0.098231837 \tag{17}$$

Therefore, the value at zero grid spacing can be computed as follows:

$$f_{h=0} \cong 326.653 + \frac{326.653 - 326.284}{2^{0.098231837} - 1} = 331.1259615 \tag{18}$$

Now GCI indices can be calculated from the below equation:

$$GCI = 1.25 * \frac{\left|\frac{f_1 - f_2}{f_{f1}}\right|}{r^p - 1} * 100\% \tag{19}$$

$$GCI_{12} = 1.25 * \frac{\left|\frac{326.653 - 326.284}{326.653}\right|}{2^{0.098231837} - 1} * 100\% = 2.004023206\% \tag{20}$$

In the same way, GCI_{23} is calculated and it equals 2.147654167%. Furthermore, it is essential to check if the GCI within the asymptotic range of convergence, however, being within the range means that the model is grid independent, which can be proved by solving the next equation:

$$\frac{GCI_{2,3}}{r^p * GCI_{1,2}} \cong 1 \qquad\qquad (21)$$

In this case, the result is 1.001130917, which means it is so close to one. Accordingly, the model is grid independent. In light of this, the medium mesh was chosen as it is proven as a reliable mesh to be considered in this study.

3.4.4 Solution methods

Patankar and Spalding, [34] created the Semi-Implicit Method for Pressure-Linked Equations (SIMPLE) algorithm, which it is used for this CFD case study. The method is fundamentally a guess-and-correct formula to calculate the pressure on the staggered grid configurations. The method considers the two-dimensional laminar steady flow correlations in Cartesian coordinates. The SIMPLE algorithm calculates pressure and velocities iteratively; when other scalars are bounded to the momentum equations, then the calculations need to be calculated consecutively [35].

3.5 Fins optimisation

FHS is predominately used as a method to cool electronic or mechanical devices, which have increased temperatures due to the operations they perform. FHS mechanisms work from the thermal conductivity of the utilized material. Clarifying this, when the air enters between the FHS, the mechanism absorbs the heat from the air, which is generally a lower temperature than the FHS, by which then conductivity initiates the cooling process of the device.

Moreover, a genetic algorithm is used to optimize the cost, the number of fins and the sizing of the geometry of the fins, i.e. spacing, height and thickness. As the genetic algorithm is defined as" a method for solving both constrained and unconstrained optimization problems based on a natural selection process that mimics biological evolution. The algorithm repeatedly modifies a population of individual solutions. At each step, the genetic algorithm randomly selects individuals from the current population and uses them as parents to produce the children for the next generation. Over successive generations, the population "evolves" toward an optimal solution"

For this case, the maximum temperature was set to be 318.15 K, which is equal to the ambient temperature, subsequently, then the total heat transfer flow was imported from the results that were obtained from ANSYS for the model of the system without fins, which will be explained in a next section. Whereas the maximum temperature permitted was set to be around 318.15K, which is the same as the ambient temperature, where the actual optimized maximum temperature from Matlab is 319.29 K.

To create a cost-effective cooling technology, the Matlab code is made to optimize the most effective geometry of fins as well as the cost of it, while the cost of PCM cannot be controlled since the desirable properties have to be met. Optimizing the cost of fins considers the efficiency of heat dissipating and the cost of the system, as they are both critical aspects and should be taken into consideration (Table 4).

Matlab code was formed regarding some equations from the open literature and implemented as explained in [36].

Table 4. Parameters of the optimized finned heat sink.

Property	Quantity	Unit
Number of fins	37	
Thickness of fins	0.002	m
Spacing between fins	0.0049	m
Fin height	0.04	m
Maximum optimized temperature at fin base	319.29	K
Cost	7.3887	£
Fin Efficiency	87.9	%

4. Results and discussion

Figure 1 shows the various temperatures on a symmetrical point (at the center) on the PV panel surface of the three models for a duration of three hours.
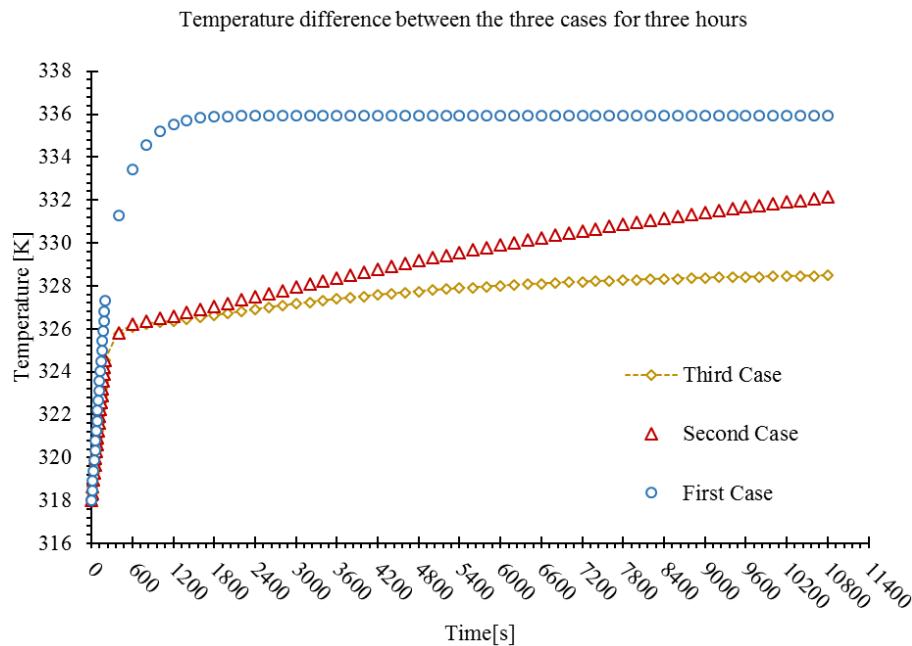

Figure 1. Three hour temperature results at the midpoint on the PV surface.

As seen in Figure 1 the trends of the temperature rise vary for each of the three cases. The temperature increase of the first case rises rapidly at the first 1600 seconds, and then becomes constant at 336 K. This is due to the extended time needed for heat to reach to the aluminium panel attached to the rear of the PV components. This assist in the dissipation of air through convection, keeping the temperature distribution in constant at the surface of the panel.

After 600 seconds, a linear pattern of the temperature growth can be seen in Figure 1 for the second case. The PCM temperature is less than the constant temperature at the boundary of the first case. Compared with the third case, as the latter two cases have displayed the same temperature during the first period of temperature rise. After this time, the PCM begins absorbing the heat, which comes from the boundary conditions and stores it in the PCM particles as LH, therefore results with slow increase of temperature. When the LH stops being extracted, meaning the PCM has been almost entirely melted, this results in a low rate of decreasing the PCM temperature, which accelerates the PV temperature. However, for the third case, the surface temperature increases slower, which is caused by the optimized fins. The functionality of fins increases the heat transfer between the PV system and the ambient conditions. Hence, the fins were optimised to dissipate the heat that comes from the container and to keep the temperature of the container as close to the ambient temperature as possible, which is almost equal to the melting point of the PCM. This suggests that it keeps the PCM absorbing the excess heat from the PV panel, and delays the time of reaching the ultimate melting point of the PCM, meaning the LH is not being conserved at this point.

Figure 2 explains the first elapsed time of operating system on the PV panel surface. The first 400 seconds are the time of transfer the heat by conductivity which mainly happens in PV panel as all cases have the same properties for this zone. It can be seen from the chart that the trend of the three models are the same, particularly for the second and third cases. Nevertheless, the abstract PV model has a higher temperature; this is due to the convection mean which effects the PV model in the same time as with conduction, due to the model being exposed to the air directly at the variance of the other two cases which they are bound by PCM.

This period divides into two regions: when the temperature rises with a smaller slope than at the beginning of the process when the PCM was relatively solid. This is due to the higher SH capacity of the liquid PCM in comparison with the SH capacity of the solid PCM [28]. Nevertheless, the front plate temperature linearly rises toward its maximum in the second case since due to the absorption process not being efficient as it was in the initial solid phase of PCM. In the third case, the PCM keeps absorbing the LH, as the

optimised fins dissipate the heat to the ambient atmosphere, which keeps the PCM at a constant temperature. The second status is the convection heat in the abstract PV model, which happens between PV panel and the ambient conditions after 400 seconds. This is also influenced by SH, a process in which absorbs a specific amount of heat per unit mass that needed to rise 1 °C, although, this process does not occur when involved with the transition phase of a material due to no temperature change despite the factors of heat being added or reduced [28]. From the initial results, the implementation of PCM shows to be a vital function to alleviate the PV temperature.
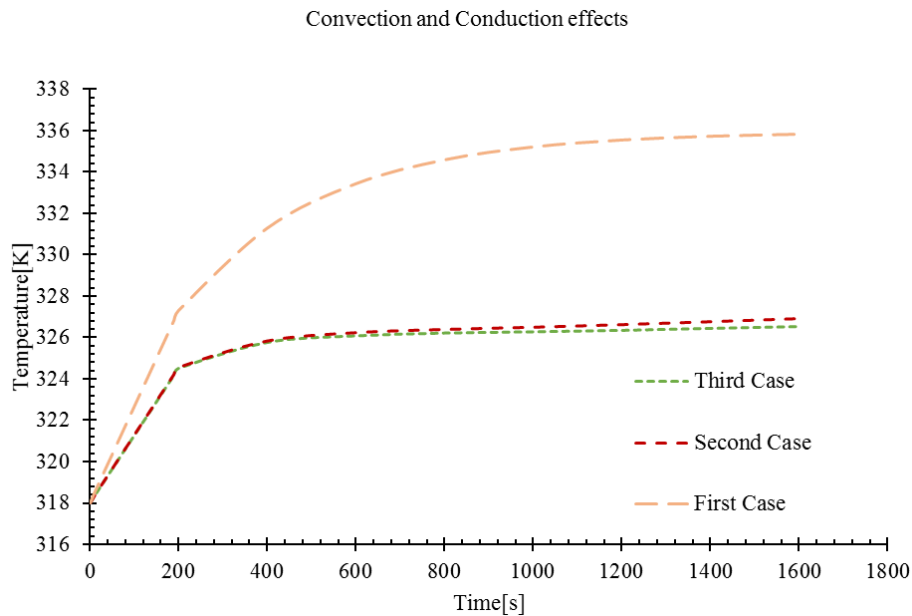
Figure 2. Temperature trends for the first period of the system operation.

Figure 3 and Figure 4 shows that the temperature differences and melting process for the second case during the tested time (three hours). Mass fraction related numerically to the solidification and melting process, as the higher mass fraction means more particles have melted. The linear trend of the PV temperature occurs from the melting process of the PCM, which occurs as a result of heat absorption from the surroundings.

Applying the optimised fins into the container of PCM has improved the reduction of temperature significantly. When the results are compared to the second case, the surface temperature decreased 4 K after 3 hours of applying the operating condition on the model, while the temperatures after one hour and two hours are 327.4 K and 328.2 K, respectively. Despite this, the trend of temperature rise is almost at a constant which is seen in Figure 1.
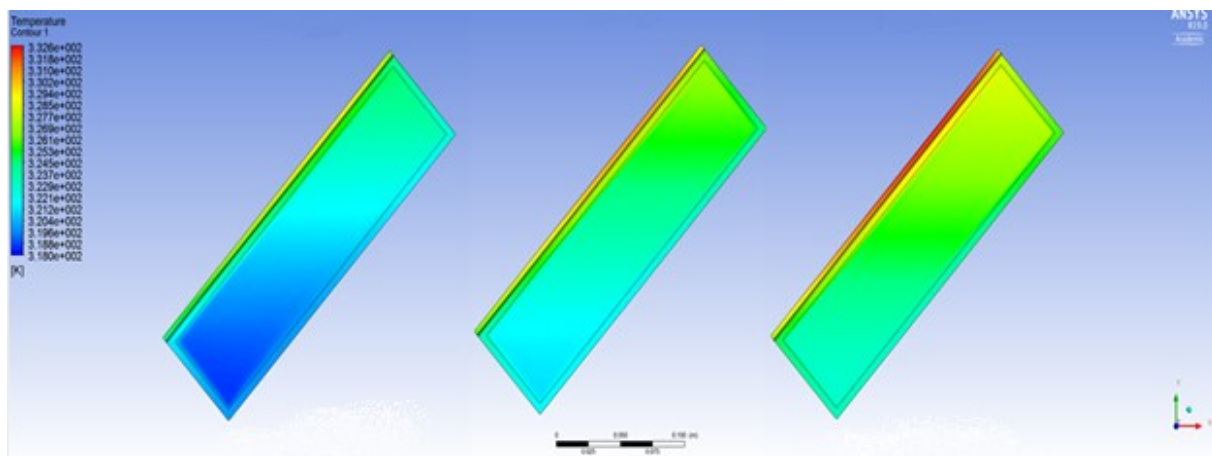

Figure 3. Temperature of PV panel and PCM model for three hours under the operating conditions. Left – hour 1, middle – hour 2, right – hour 3.
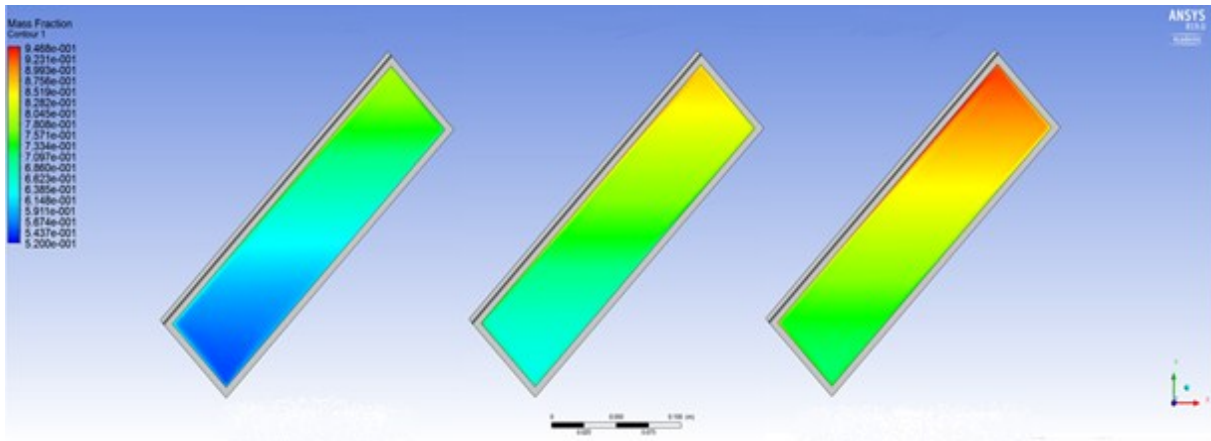
Figure 4. Melting process of PCM in the second case for three hours under the operating conditions. Left – hour 1, middle – hour 2, right – hour 3.
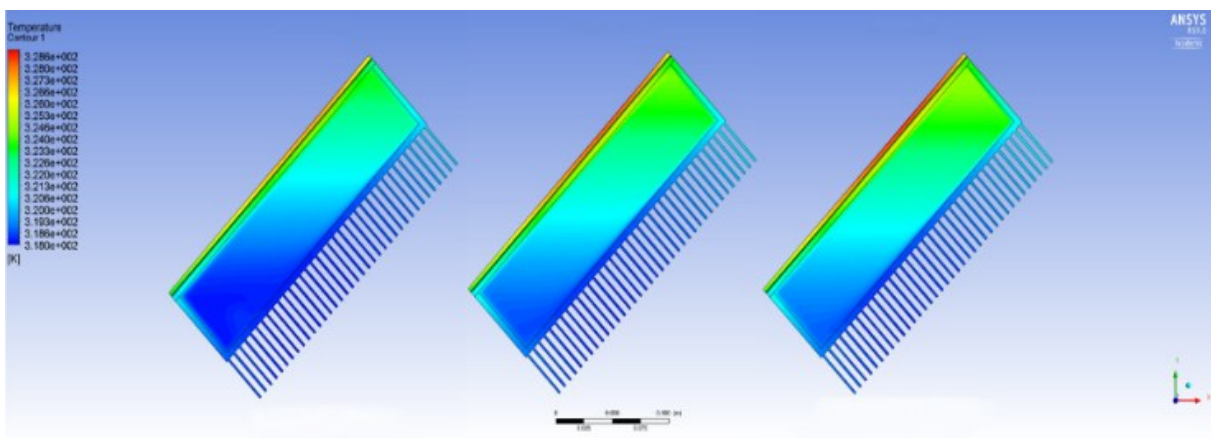

Figure 5. Temperature of the PV, PCM and optimized fins model for three hours. Left – hour 1, middle – hour 2, right – hour 3.

Figure 6 provides a visual to illustrate the longer duration of the melting process in comparison with the Second Case. This is due to the addition of the optimised fins to the model.
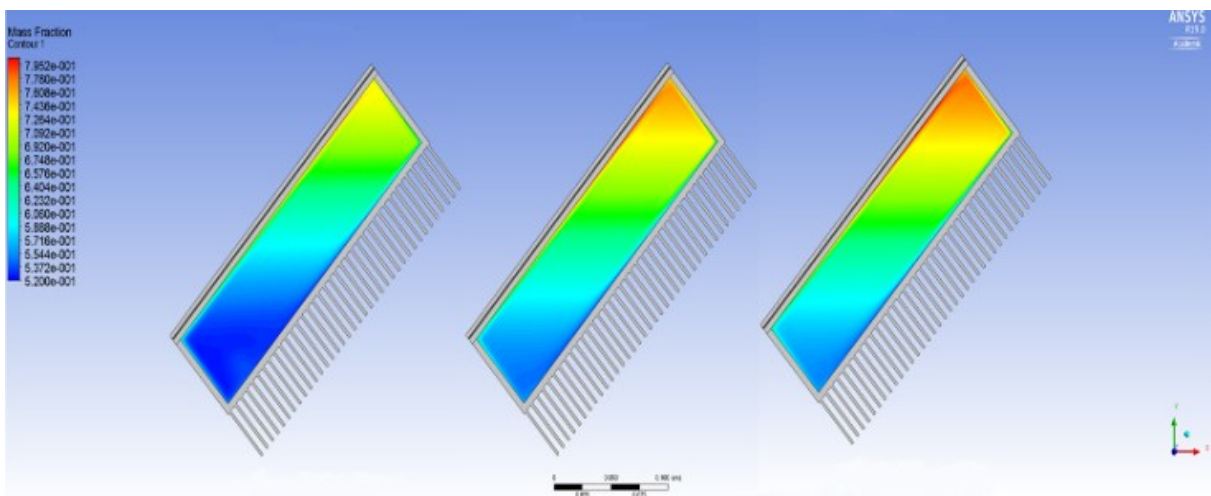

Figure 6. Melting process of PCM of the PV, PCM and optimized fins model for three hours.

To compare the second and the third case, a diagonal section of the container was sampled (Figure 7). This result is shown in Figure 8. The mass fraction of the PCM is higher on the top of the container for both cases and the whole three-hour period. This is due to the buoyancy phenomena, which induces the flow to the top of the container due to the temperature gradient resulting in a quicker melting rate of PCM in the highest point of the container in comparison with the lowest point. A thin upper layer has melted in the adjacent part of the aluminium plate at the early period, demonstrating that the conduction is the governing mean of heat transfer; afterwards, the buoyancy predominates on the surrounding nodes. The beginning of convection makes the fluid-solid interface bend, therefore boosting the melting procedure.
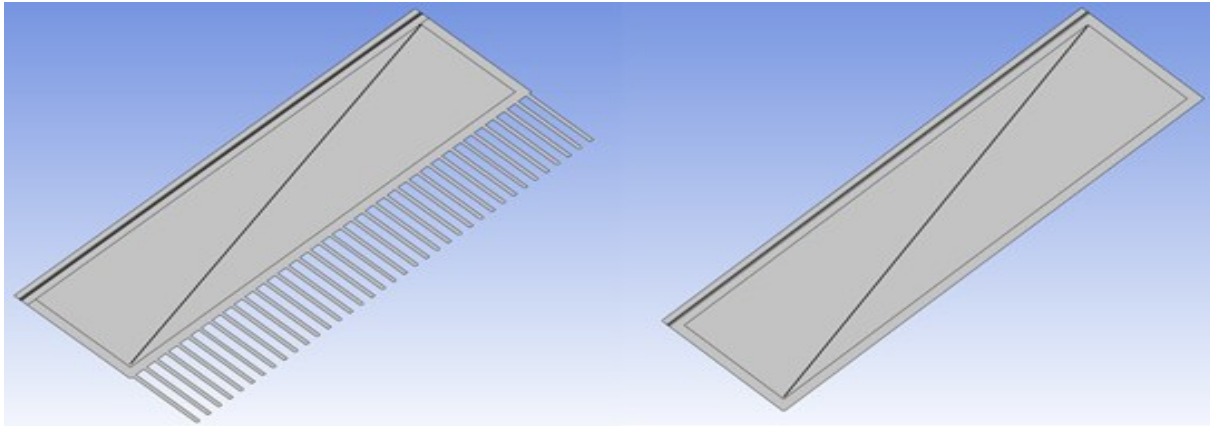

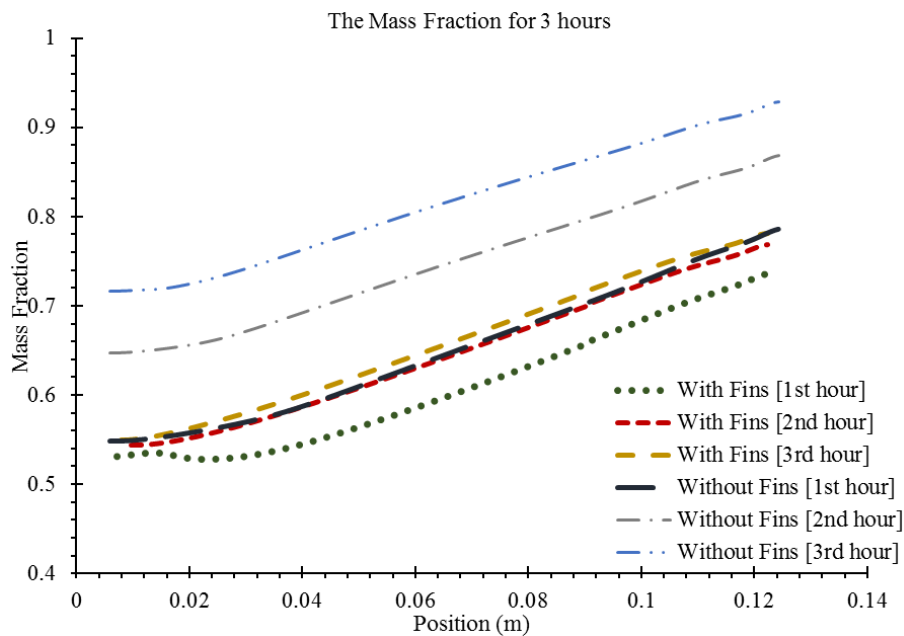Figure 7. Sample points through the container geometry.

Figure 8. The mass fraction of the PCM for the second and third cases during 3 hours.

There is a considerable difference between the temperature at the container base of the second and third case (Figure 9). The temperature increases quickly at the base of the container without fins, showing that the temperature reaches 323.7K after 3 hours of the operating time. In contrast, the container with fins increases leisurely, whereas the temperature remains around 318 K, for instance, the temperature at the end of the tested period (3 hours) reaches 318.7K. Table 5 shows the temperature drop percentage for the second and third cases in comparison with the first case.

Local temperatures were sampled on the containers of the second and third cases (Figure 10) to obtain further insight into the heat transfer and melting processes. The results of this sampling is shown in Figures 11-14.

Table 5. Temperature drop percentage of the container external base temperature in comparison with first case.

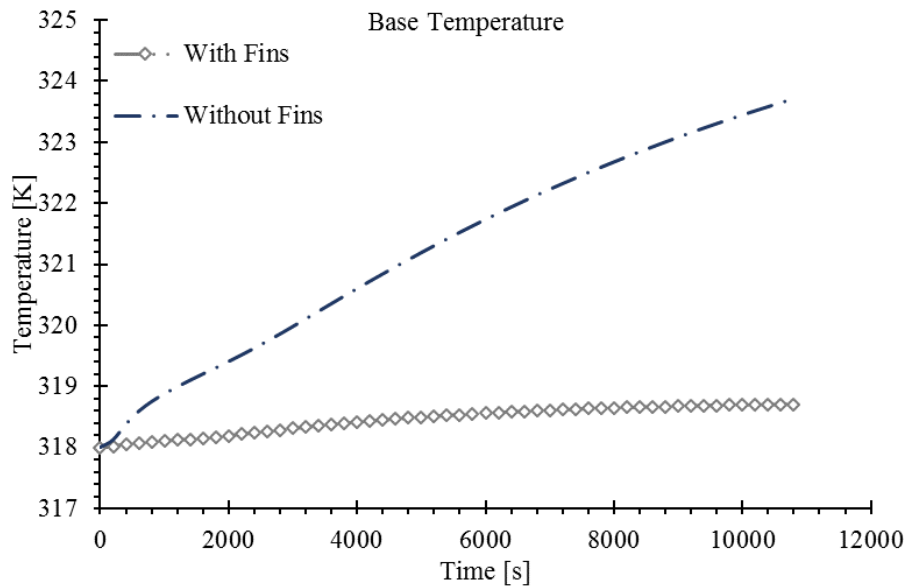| Instance	Second case	Third case
Hour 1	12.1 %	13.6 %
Hour 2	8.57 %	12.34 %
Hour 3	6.10 %	11.88 %

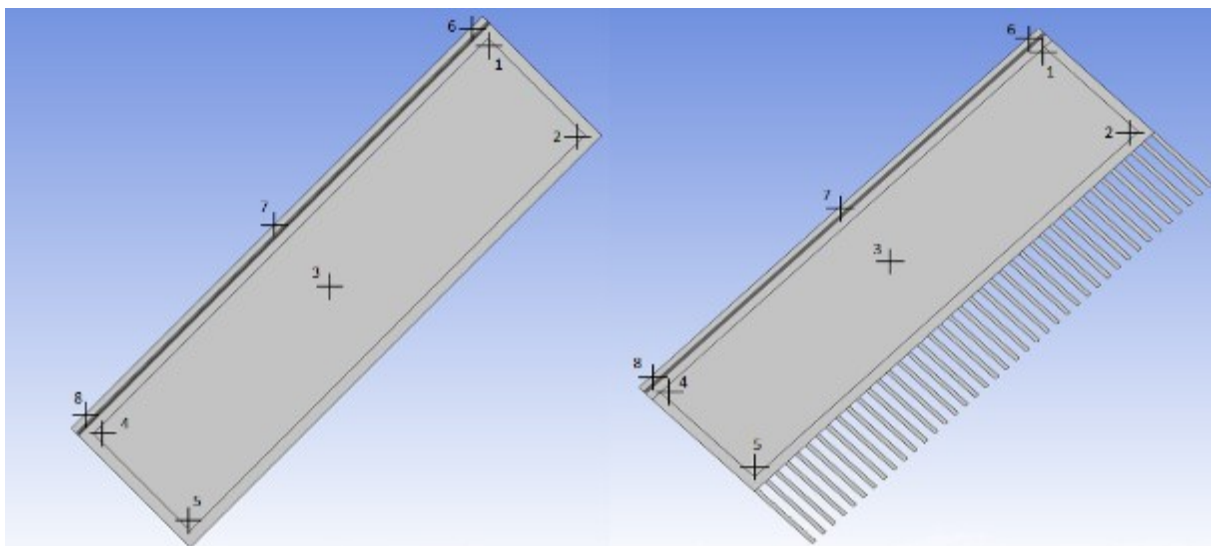Figure 9. The difference between the container base temperature with the present of fins and its absence.

Figure 10. Sample points of different positions for the second and third cases.

At the commencement of the transformation process from solid to liquid of the PCM, the rate of thermal transfer Q_{cond} is equal the enthalpy absorbed rate at the interface with aluminium plate, which can be expressed in the next equation [37].

$$Q_{cond} = Q_{lat} \tag{22}$$

This process is observed in point 1 and 4 at the early stage of the elapsed time; this is due to the dominant heat transfer method, which is conduction. The period is short due to the initial temperature being higher

than the melting point of PCM. Furthermore, conducted heat is produced from the heat flux on the PV surface and the streamline temperature on the container's walls, therefore, the melting starts immediately and rapidly in the back of the aluminium plate. This mode lasts 400 seconds, as seen in Figure 11-14. The dissimilarity of temperature is noticeable, while it is due to the driven heat to the points. As the heat in the point 1 and 4 is produced from the heat flux on the PV panel surface and the convection boundary on the sidewalls, nevertheless, point 1 temperature is higher than point 4. This is caused by the melted portion of PCM along the aluminium, which has moved to this point creating the temperature dissimilarity during this regime.

Likewise, point 2 and 5 are influenced by the conduction heat transfer as for both points the temperature trends are tied on this regime, this is observed before the period of 400 seconds. The driven heat for these points is created from the convection condition on the bottom and sidewalls. Point 3 has no change in this regime, as it is isolated by PCM.

With the progression of time (beyond 400 seconds), the melted part of PCM starts moving circularly due to the convection behaviour, resulting in a movement towards the top part of the container. The direction of PCM movement is caused by buoyancy phenomena, which induces the flow to the top of the container due to the temperature gradient. This result in a quicker melting rate of PCM in the highest point of the container in comparison with the lowest point. Gravity has an additional effect on the movement of the particles, as the density of PCM decreases with increasing the temperature. The particles with lower density (and higher temperature) go towards the top and vice versa.
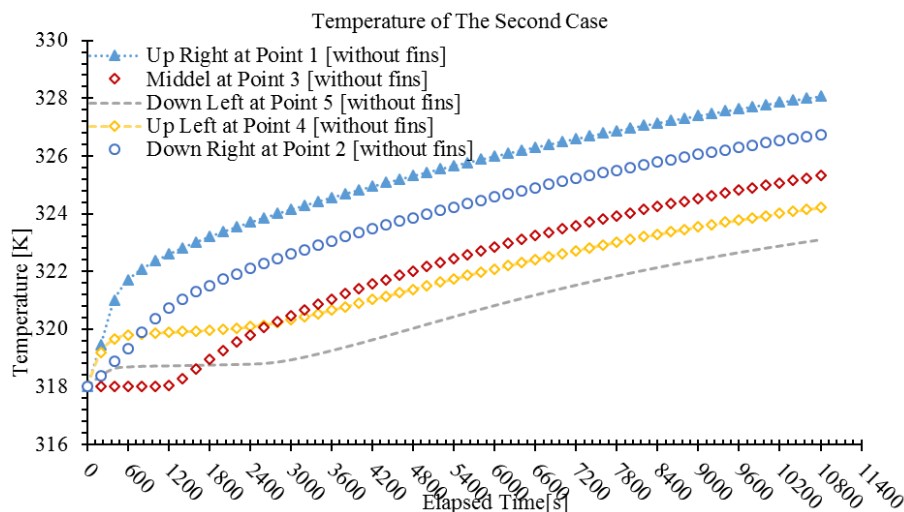

Figure 11. Temperature result at sample points in the PCM container for the second case.
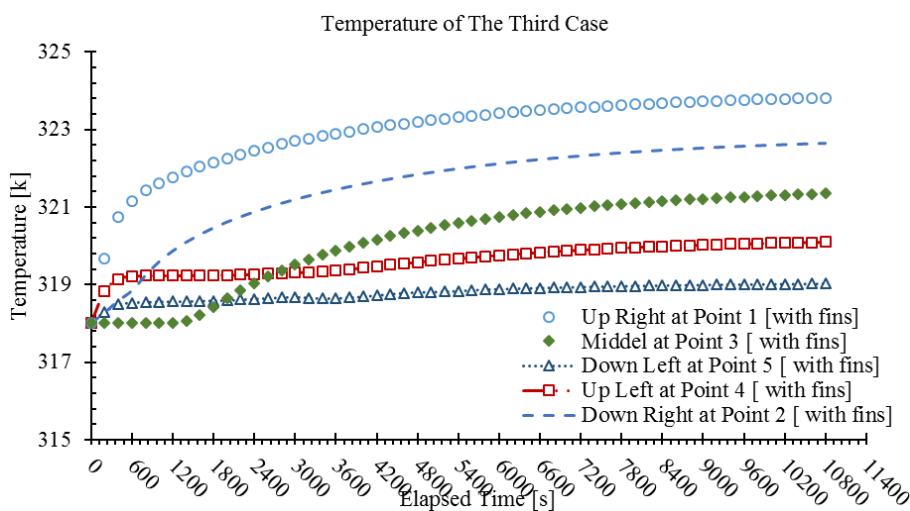

Figure 12. Temperature result at sample points in the PCM container for the third case.
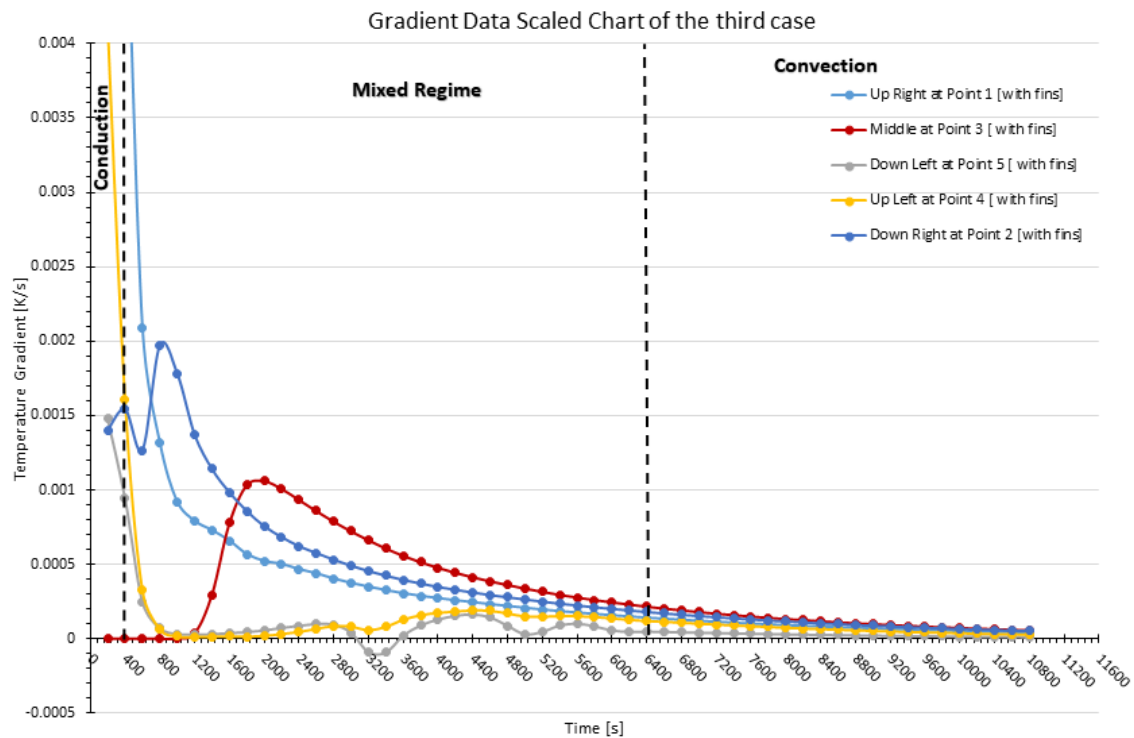
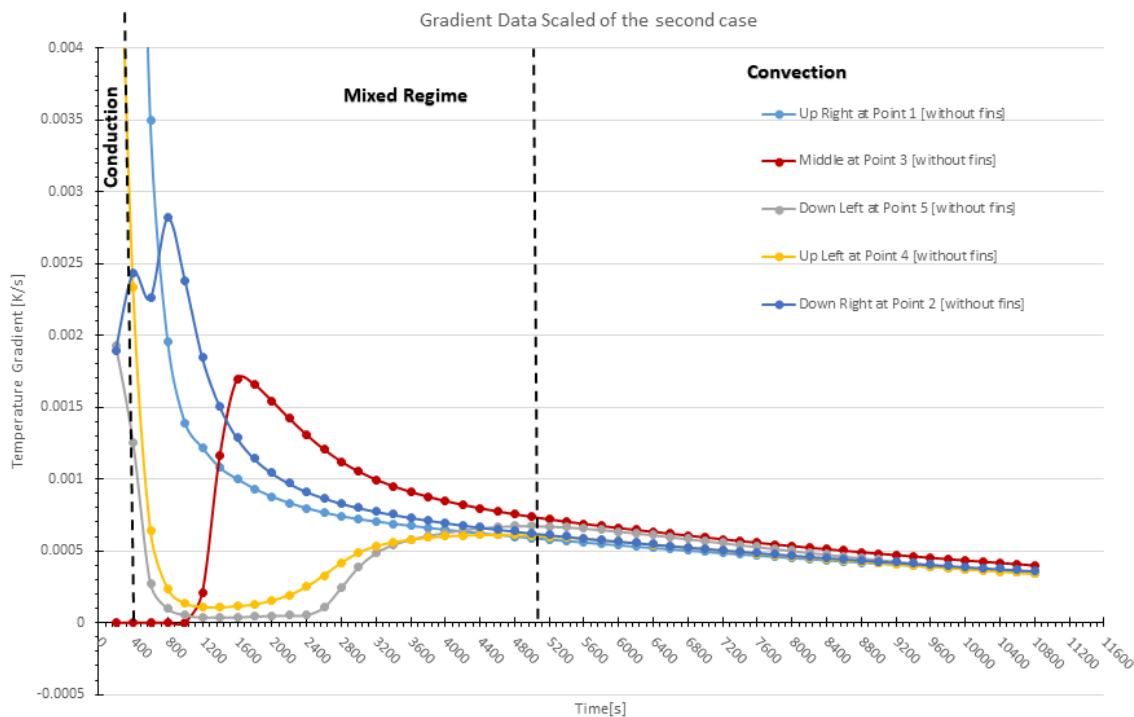Figure 13. Gradient Data Scaled Chart of the third case.

Figure 14. Gradient Data Scaled Chart of the second case.

In this region of mixed convection and conduction, the expansion of the melted PCM increases progressively due to the convection influx. This regime is applied on point 2 and 3, while the movement of the melted PCM influences them. Especially for point 3, where its mass fraction and temperature start increasing rapidly as the melted PCM moves towards the lower parts gradually due to its location. Whereas point 2 is dominated at the beginning of the operating time by the conduction heat transfer. Point 4 and 5 are dominated by the conduction mechanism.

The mixed regime lasts longer in the third case than in the second case, whereas it finishes roughly after 6400s. This is caused by the enhanced heat transfer between the PCM through the container to the ambient by applying the fins. This delays the time of the fully melted point of the PCM in the container (for the third case), meaning a longer time is needed to turn to the next regime (convection). In contrast, the second case starts this stage with the third one, but it finishes earlier (5100s), as seen in Figure 13 and Figure 14. The temperature change fluctuates and has a big gap between the points due to the method that dominates the points. For example, there was a big difference in comparison with points 1 and 2, and points 4 and 5 due to the difference in the dominant methods used. The conduction mechanism influences point 4 and 5, and convection being the main method influencing points 1 and 2. At the end of this period, the transition period finishes governing, and the convection method starts dominating.

The convection regime starts when PCM mass fraction is in-between a solid-liquid state of matter, in which the PCM is partially melted allowing it to flow freely. This enables it to extend throughout the PCM container. In this circumstance, the thickness of the mixing zone of the melted PCM becomes wider over time, inevitably dominating the entire PCM domain. Besides, the heat transfer rate is affected by the velocity of the particles in front of the surrounding walls of the container. The interface of the heat convection form is deformed because of the difference in heat penetration at the top section of the container (point 1) and the bottom (point 5). This stage starts after 6400 and 5100 seconds for the second and the third case, respectively. The gradient temperature over the PCM domain trends constantly after these times, as shown in meaning the temperature is distributed uniformly by one mean of heat transfer (convection).

When the melting process has spread over the PCM domain, some particles remain in a solid phase. Meaning the fully melted portion of PCM lessens the particles that have not been fully melted yet. The second case is more likely to be affected by this regime within a short time, whilst the third case least likely to go through this regime as the mass fraction, for all points, shows an almost constant trend towards the fully melted phase.

The melting process starts immediately as the initial temperature is higher than the melting point of PCM. Figure 15 shows the mass fraction of the third case, displaying that PCM has not been fully melted at the end of the third hour, meaning PCM is still able to absorb LH from the PV panel. The trend of the melting process indicates that the mass fraction is nearly constant and capable to mitigate the temperature for a long time. Figure 16 displays the mass fraction of the second case, the trend of PCM melting process moves rapidly in comparison with the previous case, as the mass fraction at the end of the 3 hours is 0.923, implying that PCM will melt in a short time. The much lower mass fraction of the third case (PCM with container fins) in comparison to the second case, indicates the viability of using this configuration for effective temperature management inside PV systems. In this case the effect of radiation below the system has been neglected and have to be investigated in subsequent studies.
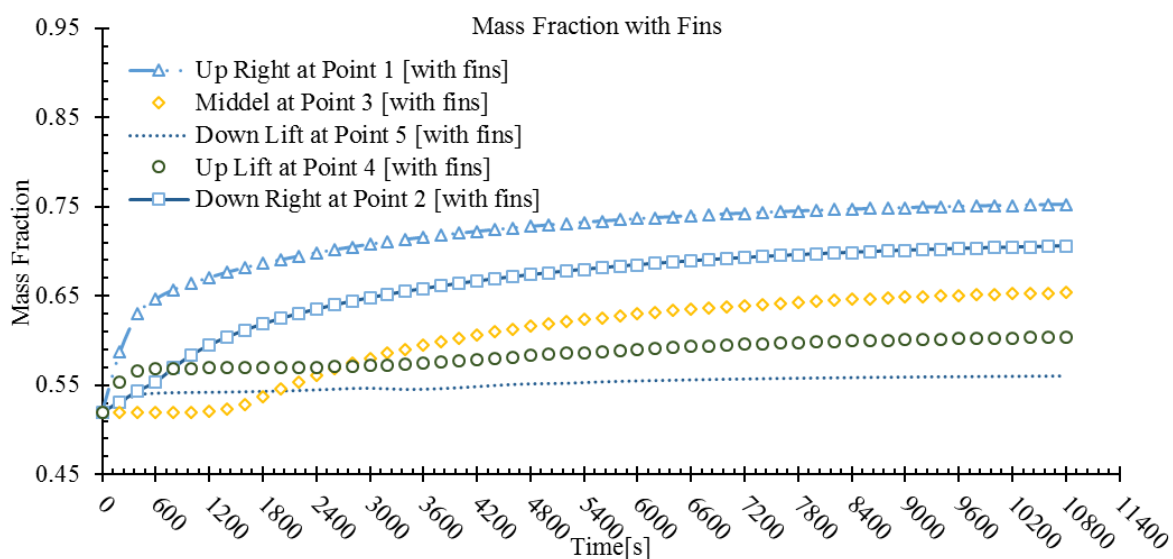

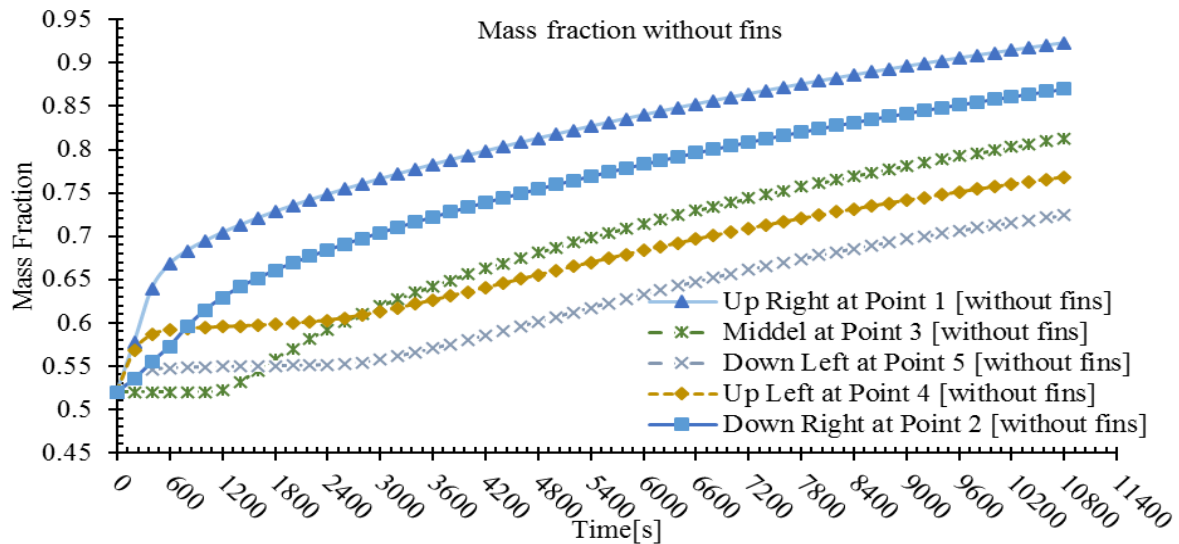Figure 15. Mass fraction of the third case.

Figure 16. Mass fraction of the second case.

5. Conclusion

In this investigation, the aim was to assess the implementation of FHS and PCM as a cooling technology for PV panel to be exploited under harsh conditions. This project was undertaken to examine three cases with different components, namely; abstract PV panel (first case), PV panel with a container contains PCM (second case) and PV panel with optimized fins applied on the PCM container (third case). These cases were used to evaluate the significant effects on the PCM before and after applying the optimized fins and to compare the results with the abstract model. The dimensions, the cost and number of fins were optimized in Matlab, as the optimization procedure considers the cost and the efficiency of the fins to make this cooling system as cost-effective as possible, while the cost of PCM is not adjustable due to the desirable properties that should be met. Accordingly, applying the fins to the container show 5K decrease in the base of the container, the cost of the fins is £7.3887, and the efficiency is 87.9%.

This study has shown that the abstract PV panel surface temperature reaches 336 K after 1600 seconds, and it maintains this temperature for the simulated three hours duration. The second case has not exceeded 332 K during the testing time. It shows a linear temperature increase the rear of the PV panel. Applying the fins in the third case shows an almost stable temperature tendency, whereas the temperature at the end of the three-hour period is almost constant at 328 K. This enhance the heat transfer between the PCM inside the container and the surrounding atmosphere.

The major finding to emerge from this study is that the optimized fins have improved the effectiveness of heat transfer between the PCM and the ambient atmosphere. This assist in the delay of the transition phase of the PCM, as the absorption process of the heat that comes from the PV surface occurs during this phase. Further investigation and experimentation into a higher PCM fusion temperature is recommended, as the present work findings show that the transition phase starts immediately after applying the boundary conditions. Whilst delaying the onset time of this phase helps absorbing more heat, consequently the temperature of PV surface will decrease. Further work could usefully explore how the solid faction/melting process performs during the natural day conditions, not just only under a fixed ambient temperature and heat flux.

References

[1] González-González, A., Jimenez Cortadi, A., Galar, D. and Ciani, L. Condition monitoring of wind turbine pitch controller: A maintenance approach. Measurement. 2018, 123, 80-93.

[2] Popovici, C. G., Hudişteanu, S. V., Mateescu, T. D. and Cherecheş, N.-C. Efficiency Improvement of Photovoltaic Panels by Using Air Cooled Heat Sinks. Energy Procedia. 2016, 85, 425-432.

[3] Tan, L. P. Passive Cooling of Concentrated Solar Cells Using Phase Change Material Thermal Storage. 2013. Doctor of Philosophy Thesis, RMIT University.

[4] Jain, K. Density and partial equivalent volumes of hydrated melts: Tetrahydrates of calcium nitrate, cadmium nitrate, and their mixtures with lithium, sodium, and potassium nitrate. J. Chem. Eng. Data. 1973, 18 (4), 397-399.

[5] Hasan, A., McCormack, S. J., Huang, M. J. and Norton, B. Evaluation of phase change materials for thermal regulation enhancement of building integrated photovoltaics', Solar Energy. 2010, 84(9), 1601-1612.

[6] Ahmed, R. and Nabil, K. A. I. Computational analysis of phase change material and fins effects on enhancing PV/T panel performance. Journal of Mechanical Science and Technology. 2017, 31(6), 3083-3090.

[7] Ma, T., Yang, H., Zhang, Y., Lu, L. and Wang, X. Using phase change materials in photovoltaic systems for thermal regulation and electrical efficiency improvement: A review and outlook. Renewable and Sustainable Energy Reviews. 2015, 43, 1273-1284.

[8] Siecker, J., Kusakana, K. and Numbi, B. P. A review of solar photovoltaic systems cooling technologies. Renewable and Sustainable Energy Reviews. 2017, 79, 92-203.

[9] Tonui, J. K. and Tripanagnostopoulos, Y. Improved PV/T solar collectors with heat extraction by forced or natural air circulation. Renewable Energy. 2007, 32(4), 623-637.

[10] Linan, J., Mikkelsen, J., Jae-Mo, K., Huber, D., Shuhuai, Y., Lian, Z., Peng, Z., Maveety, J. G., Prasher, R., Santiago, J. G., Kenny, T. W. and Goodson, K. E. Closed-loop electroosmotic microchannel cooling system for VLSI circuits. IEEE Transactions on Components and Packaging Technologies. 2002, 25(3), 347-355.

[11] Kane A. and Verma V. Performance Enhancement of Building Integrated Photovoltaic Module using Thermoelectric Cooling. International J. of Renewable Energy Research-IJRER. 2013, 3(2).

[12] R. Hosseini, N. Hosseini and Khorasanizadeh H. An experimental study of combining a photovoltaic system with a heating. World Renewable Energy Congress. 8-13 May 2011. Linköping, Sweden.

[13] Sharma A., Tyagi V.V., Chen C.R., Buddhi D. Review on thermal energy storage with phase change materials and applications. Renewable and Sustainable Energy Reviews. 2009, 13(2), 318-345.

[14] Hausler T. and Rogass H. Photovoltaic module with latent heat storage –collector. Proceedings of the 2nd world conference and exhibition on Photovoltaic solar energy conversion. 6-10 July 1998, Vienna.

[15] Huang, M. J., Eames, P. C. and Norton, B. Chapter 454 - The Application of Computational Fluid Dynamics to Predict the Performance of Phase Change Materials for Control of Photovoltaic Cell Temperature in Buildings, Sayigh, A.A.M. (ed.). World Renewable Energy Congress VI. Oxford: Pergamon, 2000, pp 2123-2126.

[16] Ibrahim, N. I., Al-Sulaiman, F. A., Rahman, S., Yilbas, B. S. and Sahin, A. Z. Heat transfer enhancement of phase change materials for thermal energy storage applications: A critical review. Renewable and Sustainable Energy Reviews, 2017, 74, 26-50.

[17] Huang, M. J., Eames, P. C. and Norton, B. Phase change materials for limiting temperature rise in building integrated photovoltaics. Solar Energy. 2006, 80(9), 1121-1130.

[18] Velraj, R., Seeniraj, R. V., Hafner, B., Faber, C. and Schwarzer, K. Experimental analysis and numerical modelling of inward solidification on a finned vertical tube for a latent heat storage unit. Solar Energy. 1997, 60(5), 281-290.

[19] Ismail, K. A. R., Alves, C. L. F. and Modesto, M. S. Numerical and experimental study on the solidification of PCM around a vertical axially finned isothermal cylinder. Applied Thermal Engineering. 2001, 21(1), 53-77.

[20] Chan Choi, J., Done Kim, S. and Young Han, G. Heat transfer characteristics in low-temperature latent heat storage systems using salt-hydrates at heat recovery stage. Solar Energy Materials and Solar Cells. 1996, 40(1), 71-87.

[21] Stritih, U. An experimental study of enhanced heat transfer in rectangular PCM thermal storage. International Journal of Heat and Mass Transfer. 2004, 47(12), 2841-2847.

[22] Rahimi, M., Ranjbar, A. A., Ganji, D. D., Sedighi, K., Hosseini, M. J. and Bahrampoury, R. Analysis of geometrical and operational parameters of PCM in a fin and tube heat exchanger. International Communications in Heat and Mass Transfer. 2014, 53, 109-115.

[23] Xu, S., Wang, W., Fang, K. and Wong, C.-N. (2015) 'Heat transfer performance of a fractal silicon microchannel heat sink subjected to pulsation flow', International Journal of Heat and Mass Transfer, 81, pp. 33-40.

[24] Yu, Y., Simon, T. and Cui, T. A parametric study of heat transfer in an air-cooled heat sink enhanced by actuated plates. International Journal of Heat and Mass Transfer. 2013, 64, 792-801.

[25] Li, H.-Y., Chiang, M.-H., Lee, C.-I., Yang, W.J. Thermal performance of plate-fin vapor chamber heat sinks. International Communications in Heat and Mass Transfer. 2010, 37(7), 731-738.

[26] Lin, S.-C., Chuang, F.-S. and Chou, C.A.Experimental study of the heat sink assembly with oblique straight fins. Experimental Thermal and Fluid Science. 2005, 29(5), 591-600.[25

[27] Hasan, M. I. Investigation of flow and heat transfer characteristics in micro pin fin heat sink with nanofluid. Applied Thermal Engineering. 2014, 63(2), 598-607.

[28] Biwole, P. H., Eclache, P. and Kuznik, F. Phase-change materials to improve solar panel's performance. Energy and Buildings. 2013, 62, 59-67.

[29] Khanna, S., Reddy, K. S. and Mallick, T. K. Optimization of solar photovoltaic system integrated with phase change material. Solar Energy. 2018, 63, 591-599.

[30] Angell, C. A. and Tucker, J. C. Heat capacities and fusion entropies of the tetrahydrates of calcium nitrate, cadmium nitrate, and magnesium acetate. Concordance of calorimetric and relaxational ideal glass transition temperatures. The Journal of Physical Chemistry. 1974, 78(3), 278-281.

[31] Egorov, B.N., Revykina, M.P., Trokhinin, N.N., Trushevskii, S.N. and Fedorova, T.M. Investigation of crystal hydrates thermophysical properties in respect to heat storage problems. Solar energy. 1979, 16(3), 61-64.

[32] Kenisarin, M. and Mahkamov, K. Salt hydrates as latent heat storage materials: Thermophysical properties and costs. Solar Energy Materials and Solar Cells. 2016, 145, 255-286.

[33] Brent, A. D., Voller, V. R. and Reid, K. J. Enthalpy-porosity technique for modeling convection-diffusion phase change: application to the melting of a pure metal. Numerical Heat Transfer. 1988, 13(3), 297-318.

[34] Patankar, S.V. and Spalding, D.B. A Calculation Procedure for Heat, Mass and Momentum Transfer in Three-Dimensional Parabolic Flows. International Journal of Heat and Mass Transfer. 1972, 15, 1787-1806.

[35] Versteeg, H. K. and Malalasekera, W. An Introduction to Computational Fluid Dynamics. 2007, Edinburgh, England: Pearson Education Limited.

[36] Currie I. G. Fundamental Mechanics of Fluids. 2003, 3rd Edition, Marce-Dekker, New York.

[37] Al-Jethelah, M., Humaira Tasnim, S., Mahmud, S. and Dutta, A. Melting of nano-PCM in an enclosed space: Scale analysis and heatline tracking. International Journal of Heat and Mass Transfer. 2018, 119, 841-859.

[38] Slater,J.W. Examining Spatial (Grid) Convergence. 2008, https://www.grc.nasa.gov/www/wind/valid/tutorial/spatconv.html.

Ahmad Elamaireh obtained his Bachelor's degree in Mechanical Engineering in 2016 from Mutah University, Jordan. He completed an Engineering Master's degree in Renewable Energy and Sustainable Development from Northumbria University in 2018. He is a specialist in solar panel technology and applications for desert regions.
E-mail address: ahmad.elamaireh@northumbria.ac.uk

Jaydeep Goraniya holds a Bachelor's degree in Electrical Engineering from Charotar University of Science and Technology, India. He is currently completing an Engineering Master's degree in Renewable Energy and Sustainable Development from Northumbria University.
E-mail address: jaydeep.goraniya@northumbria.ac.uk

Madeleine L Combrinck holds a B.Eng Mechanical Engineering (2006) and a M.Sc Mechanical Engineering (2009) both from Stellenbosch University, South Africa, and obtained a PhD in 2017 from the University of Pretoria, South Africa. She specialises in Computational Fluid Mechanics and Numerical Methods. Her research interests relates to utilizing modelling and simulation techniques to gain insight into real world problems ranging from defense applications to renewable and sustainable energy solutions.
E-mail address: madeleine.combrinck@northumbria.ac.uk